Natural quasy-periodic binary structure with focusing property in near field diffraction pattern

Mona Mihailescu

"Politehnica" University from Bucharest, Physics Department, 313 Splaiul Independentei 060042,Bucharest, Romania

mona_m@physics.pub.ro

Abstract: A naturally-inspired phase-only diffractive optical element with a circular symmetry given by a quasi-periodic structure of the phyllotaxis type is presented in this paper. It is generated starting with the characteristic parametric equations which are optimal for the golden angle interval. For some ideal geometrical parameters, the diffracted intensity distribution in near-field has a central closed ring with almost zero intensity inside. Its radius and intensity values depend on the geometry or non-binary phase distribution superposed onto the phyllotaxis geometry. Along propagation axis, the transverse diffraction patterns from the binary-phase diffractive structure exhibit a self-focusing behavior and a rotational motion.

OCIS codes: (050.1940) Diffraction; (050.1970) Diffractive optics, (170.1420) Biology.

References and links

1. A. J. Caley, M. J. Thomson, J. Liu, A. J. Waddie, M. R. Taghizadeh, "Diffractive optical elements for high gain lasers with arbitrary output beam profiles," Opt. Express **15**(17), 10699-10704 (2007). http://www.opticsinfobase.org/oe/abstract.cfm?URI=oe-15-17-10699
2. G. S. Khan, K. Mantel, I. Harder, N. Lindlein, J. Schwider, "Design considerations for the absolute testing approach of aspherics using combined diffractive optical elements," Appl. Opt. **46**(28), 7040-7048 (2007) http://www.opticsinfobase.org/abstract.cfm?URI=ao-46-28-7040
3. H. Angelskår, I.-R. Johansen, M. Lacolle, H. Sagberg, A. S. Sudbø, "Spectral uniformity of two- and four-level diffractive optical elements for spectroscopy," Opt. Express **17**(12), 10206-10222 (2009). http://www.opticsinfobase.org/oe/abstract.cfm?URI=oe-17-12-10206
4. G. Mínguez-Vega, O. Mendoza-Yero, J. Lancis, R. Gisbert, P. Andrés, "Diffractive optics for quasi-direct space-to-time pulse shaping," Opt. Express, **16**(21), 16993-16998 (2008) . http://www.opticsinfobase.org/oe/abstract.cfm?URI=oe-16-21-16993
5. A.R. Moradi, E. Ferrari, V. Garbin, E. Di Fabrizio, D. Cojoc, "Strength control in multiple optical traps generated by means of diffractive optical elements", J. Opt. Adv. Mat. RC, **1**(4) 158-161, (2007).
6. C. Iemmi, J. Campos, J. C. Escalera, O. López-Coronado, R. Gimeno and M. J. Yzuel, "Depth of focus increase by multiplexing programmable diffractive lenses", Opt. Express **14**(22), 10207-10219 (2006). http://www.opticsinfobase.org/oe/abstract.cfm?URI=oe-14-22-10207
7. K. Kimura, S. Hasegawa and Y. Hayasaki, "Diffractive spatiotemporal lens with wavelength dispersion compensation," Opt. Lett. **35**(2), 139-141 (2010) , http://www.opticsinfobase.org/ol/abstract.cfm?URI=ol-35-2-139
8. O. Mendoza-Yero, G. Mínguez-Vega, M. Fernández-Alonso, J. Lancis, E. Tajahuerce, V. Climent, and J. A. Monsoriu, "Optical filters with fractal transmission spectra based on diffractive optics," Opt. Lett. **34**(5), 560-562 (2009). http://www.opticsinfobase.org/ol/abstract.cfm?URI=ol-34-5-560
9. N. Ferralis, R.D. Diehl, "Diffraction from one- and two-dimensional quasicrystalline gratings", Am. J. of Phys. Volume 72(9), 1241-1246 (2004). http://dx.doi.org/10.1119/1.1758221
10. M. Mihailescu, A. M. Preda, A. Sobetkii, A.C. Petcu, "Fractal-like diffractive arrangement with multiple focal points", Opto-Electr. Rev. **17**(4), 330–337 (2009)
11. N, D. Lai, J. H. Lin, and C. C. Hsu, "Fabrication of highly rotational symmetric quasi-periodic structures by multiexposure of a three-beam interference technique," Appl. Opt. **46**(10), 5645-5648 (2007) http://www.opticsinfobase.org/ao/abstract.cfm?URI=ao-46-23-5645
12. J. Duparré, P. Dannberg, P. Schreiber, A. Bräuer, and A. Tünnermann, "Artificial Apposition Compound Eye Fabricated by Micro-Optics Technology," Appl. Opt. **43**(22), 4303-4310 (2004) http://www.opticsinfobase.org/ao/abstract.cfm?URI=ao-43-22-4303

13. L. P. Biró, Z. Bálint, K. Kertész, Z. Vértesy, G. I. Márk, Z. E. Horváth, J. Balázs, D. Méhn, I. Kiricsi, V. Lousse, and J.-P. Vigneron, "Role of photonic-crystal-type structures in the thermal regulation of a Lycaenid butterfly sister species pair", Phys. Rev. E, 67**,** 021907 (2003)
14. D. Radtke, J. Duparré, U. D. Zeitner, and Andreas Tünnermann, "Laser lithographic fabrication and characterization of a spherical artificial compound eye," Opt. Express 15(6), 3067-3077 (2007), http://www.opticsinfobase.org/oe/abstract.cfm?URI=oe-15-6-3067
15. J. Rosen and D. Abookasis, "Seeing through biological tissues using the fly eye principle," Opt. Express 11(26), 3605-3611 (2003). http://www.opticsinfobase.org/oe/abstract.cfm?URI=oe-11-26-3605
16. S. -P. Simonaho and R. Silvennoinen, "Sensing of wood density by laser light scattering pattern and diffractive optical element based sensor," J. Opt. Technol. **73**(3) 170-174 (2006) http://www.opticsinfobase.org/JOT/abstract.cfm?URI=JOT-73-3-170
17. R. Todd Lee and G. S. Smith, "Detailed electromagnetic simulation for the structural color of butterfly wings," Appl. Opt. **48**(21), 4177-4190 (2009) http://www.opticsinfobase.org/ao/abstract.cfm?URI=ao-48-21-4177
18. I. R. Hooper, P. Vukusic, and R. J. Wootton, "Detailed optical study of the transparent wing membranes of the dragonfly Aeshna cyanea," Opt. Express **14**(11), 4891-4897 (2006) http://www.opticsinfobase.org/oe/abstract.cfm?URI=oe-14-11-4891
19. A. R. Parker, H. E. Townley, "Biomimetics of photonic nanostructure" Nature Nanotech. **2**(6), 347-353, 2007
20. P. Prusinkiewicz, A. Lindenmayer, "The Alogirthmic Beauty of Plants" (Springer-Verlag, New York, 1990)
21. R. O. Erickson. "The geometry of phyllotaxis" in *The growth and functioning of leaves* J. E. Dale and F. L. Milthrope, ed. pages 53–88. (University Press, Cambridge, 1983).
22. R. V. Jean. "Mathematical modelling in phyllotaxis: The state of the art", Mathem. Biosci., **64**(1) 1–27, (1983).
23. S. S. Liaw, "Phyllotaxis: Its geometry and dynamics" Phys. Rev. E, **57**, 4589 (1998).
24. L. S. Levitov, "Fibonacci numbers in botany and physics: Phyllotaxis", J. Exp. Theor. Phys. Lett. **54**(9), 546-550 (1991).
25. S. Douady, Y. Couder "Phyllotaxis as a physical self-organized growth process" Phys. Rev. Lett. **68**(13) 2098–2101 (1992).
26. G. P. Bernasconi, J. Boissonade, "Phyllotactic order induced by symmetry breaking in advanced Turing patterns", Phys. Lett., **232**(3-4), 224-230 (1997).
27. C. Nisoli, "Spiraling solitons: A continuum model for dynamical phyllotaxis of physical systems", Phys Rev. E **80**, 026110 (2009)
28. A. Murthy "Mathematics of nature and nature of mathematics" Chapter I, http://www.scribd.com/doc/21990600/Maths-of-Nature-and-Nature-of-Maths-Chapter-1
29. M. Mihailescu, A.M. Preda, D. Cojoc, E. Scarlat, L. Preda, "Diffraction pattern from a phyllotaxis type arrangement", Opt. Las. Eng., **46**(11), 802–809 (2008).
30. H.Vogel, "A better way to construct the sunflower head", Math. Biosci., **44**(3-4),179-189 (1979).
31. J. W. Goodman, "Introduction to Fourier optics", Mc Graw-Hill Book Company, 1968;
32. J. Garcia, D. Mas, R. G. Dorsch, "Fractional-Fourier-transform calculation through the fast-Fourier-transform algorithm", Appl. Opt. **35**(35), 7013-7018, (1996) http://www.opticsinfobase.org/ao/abstract.cfm?URI=ao-35-35-7013

1. Introduction

So far, in literature there were introduced, many types of diffractive elements used in different applications: in order to generate certain desired intensity distribution [1], to test aspherical surfaces [2], for near infrared spectroscopy [3], for pulse shaping in the femtosecond regime [4] to trap multiple micro-particles [5], to extend the depth of focus [6], to generate an ultrashort laser pulse and to compensate the dispersion phenomenon [7], as well as for optical filters [8]. Some quasi-periodic structures are also important like diffractive elements [9-11].

The interaction of light with systems which are designed after natural models was widely studied [12-16]. Many natural structures with peculiar optical properties [17, 18] were, also, investigated in the photonics engineering. Scientists developed many precise photonic devices, but similar properties one can also find in the natural objects which are not well enough known. Natural components from plants and animals can function like 1D diffraction gratings, multilayer deflectors or filters, 2-D and 3-D photonic crystals. Not only the composition of these natural specimens is important, but also their arrangement. Using

different techniques (lithography, reactive ion etching), scientists have already made artificial analogues [19].

Some plants lateral organs present a quasi-periodic arrangement around a central axis, of the phyllotaxis type with the golden angle interval (leaves on a stem, scales on a cone axis, florets in a composite flower head [20]). This geometry generated interest for biologists and mathematicians, reviewed by Erickson [21] and Jean [22] and more recently inspired physicists [23-27]. There are many examples from nature, regarding the phyllotaxis geometry, which represents the ordering in many plants in planar or cylindrical models (e.g. sunflower head, daisy capitulum, pinecone, pineapple). One example is the compact arrangement of the sunflower seeds (at golden angle interval) to optimize the light of which each seed is exposed to. An interesting aspect here is also the minimization of the shadow from a singular seed on the surrounding seeds. Another example is the arrangement of the leaves orientated towards the golden angle to optimize their exposed area to the falling rain (the rain is directed back along the leaf and down the stem to the roots [28]). For the purpose of mathematical analysis, their shape is reduced to a simple geometric figure, usually a circle.

A binary phase-only diffractive optical element with the structure inspired from a natural arrangement is studied here. Its geometry is computed using algebraic equations with an angle parameter. In this kind, some quasi-periodic phyllotaxis-type diffractive optical elements (PtDOEs) with a geometry containing hundreds of circular elements (CEs) arranged at the golden angle interval, on several spirals are generated like a binary phase-only diffractive optical elements.

The analysis of their near-field diffraction pattern distinguishes some features: an annular symmetry, a central closed ring (CCR) with almost zero intensity inside, a self-focusing behaviour and a rotational motion of the intensity distribution with the axial distance. This hybrid axial behaviour is useful in the multiple-plane optical tweezers at microscopic scale. To improve some desired properties of the diffraction patterns, a proper non-binary phase distribution is spatially superposed onto the PtDOE structure.

Its far-field diffraction pattern was studied elsewhere [29] considering different values for the parameters which generate the phyllotaxis geometry. There are certain values for the parameters which give in the same time the smallest intensity in zero diffraction order and the highest intensity in the first one.

2. Diffractive structures design

The mathematical models which generate the phyllotaxis geometry are related to the packing problems. The algebraic equations based on parameters n and φ build phyllotaxis geometry of n elements with the angle interval φ between two successive elements. It was demonstrated by Vogel [30] that $\varphi = \varphi_g = 137.51^o$, the golden angle, represents an optimum value to maximize the number of elements which fill a given surface. The critical role of the angle interval value φ is illustrated in the Fig. 1.

Our diffractive element consists of identical individual circular elements CE of radius r, disposed in spirals as shown in the Fig. 1. The numbers of spirals in direct and inverse trigonometric sense are two consecutive Fibonacci numbers. Here, in the design of PtDOE, it was considered only the direct trigonometric sense. The location of the n^{th} CE is given by the Cartesian coordinates (x_n, y_n) of its centre. To define them, were used the parametric equations introduced by Vogel [30]:

$$x_n = c\sqrt{n}\cos(n\varphi), \quad y_n = c\sqrt{n}\sin(n\varphi) \tag{1}$$

where $c\sqrt{n} = \rho_n$ is the distance between the centre of the n^{th} CE and the centre of the PtDOE, c is a constant scaling parameter linked with the filling factor, named here the filling interval.

$n\varphi = \varphi_n$ is the angle between a reference direction and the position vectors of the centre of each CE in a polar coordinate system (ρ_n, φ_n) originating in the centre of the PtDOE.

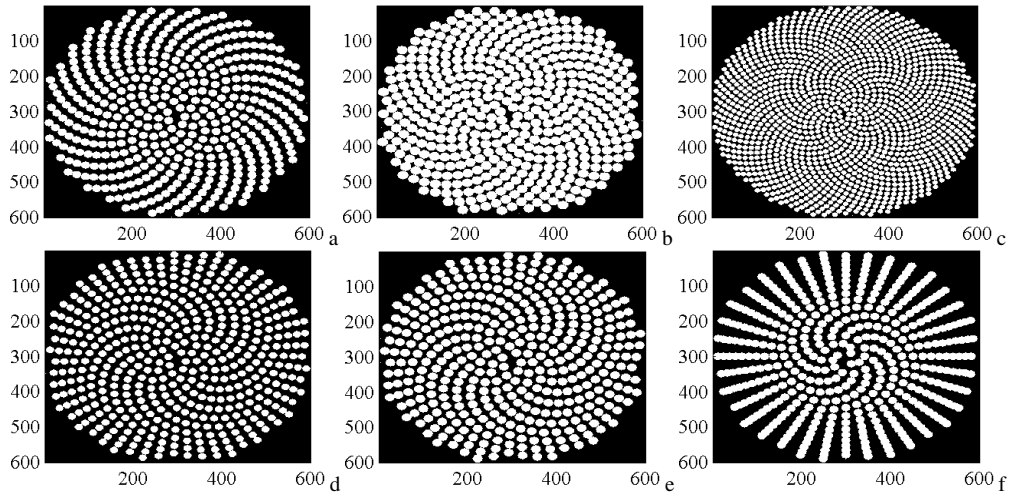

Fig. 1. PtDOEs generated with different geometrical parameters a) φ =137.55° n=459 c=14 r=10, b) φ =137.51° n=467 c=14 r=12, c) φ =137.51° n=1414 c=8 r=6, d) φ =137.45° n=470 c=14 r=9, e) φ =137.45° n=401 c=15 r=11, f) φ =130.00° n=458 c=14 r=10

Firstly, the centre of each CE is calculated and counted (n). For a different angle interval φ, this total number n is different, in the same area (see Fig. 1). For the optimum value $\varphi = \varphi_g = 137.51^o$, the number, n, can be increased, through the decreases in the c and r values (compare Fig. 1 b and c). For the same filling interval c, the total number n varies with the angle interval. There are different angles where the total number n is bigger than the number for the ideal arrangement (see Fig. 1b), but to avoid the overlapping of CE we must decrease their radius r (see Fig. 1d). In these conditions, in order to keep the same radius r, we must increase, also, the filling interval, c (see Fig. 1e), which leads to a drastic decrease in the value of n. When the values of the angle interval are far from the golden angle, the arrangement is also far from the ideal one with many overlapping CEs at the same r (see Fig. 1f).

For a given circular area of the diffractive structure, an arrangement in the phyllotaxis geometry at the golden angle has 467 CEs compared to an array of lines and columns which has 357 CEs. Defining the filling factor like a ratio between the area occupied with CEs (avoiding overlapping) and the whole area, its values for the PtDOEs from the Fig. 1, are: a) 51.0% b) 74.72% c) 56.56% d) 42.30% e) 52.11% f) 18.32%.

One can easily observe in the Fig 1, the value of the angle φ was modified from the optimum value (Fig 1b and c) to different values (Fig. 1 a, d, e, f) with major changes in the CE positions and in the filling factor value for the same area. At the ideal angle interval $\varphi = \varphi_g = 137.51^o$, for the other parameters there are several pairs of values that match with higher values of the filling factor. One example is shown in the Fig. 1b for c=14 and r=12 and the other is shown in the Fig. 1c for c=8 and r=6. If one needs to increase the value of the CE radius, r, he must increase also the filling interval c, in order to avoid the overlapping.

In the following, the PtDOE structure will be considered as a binary phase-only diffractive element in a circular aperture with the radius R_i with the transmittance function:

$$t(x, y) = \exp(i\pi\Phi(x, y)) \tag{2}$$

where the phase function, $\Phi(x, y)$, is a binary one and is determined with respect to the parametric equations (1), for different values of the parameters: c, n, φ and the radius r of the CE.

A non-binary phase distribution, $\Phi_{nb}(x, y)$, generated on the computer, is simply superposed on the PtDOE transmission function:

$$t_{nb}(x, y) = \exp(i\pi \cdot \Phi(x, y) + \Phi_{nb}(x, y)) \tag{3}$$

For example, in Fig. 2a is shown the phase distribution of the PtDOE with a lens superposed in each CE. In Fig. 2b, on the PtDOE is superposed a vortex map characterized by the azimuthal variation of the phase given in the form $\Phi_{nb} = im\phi$ where *m* is a non zero integer called the topological charge and ϕ is the azimuthal angle.

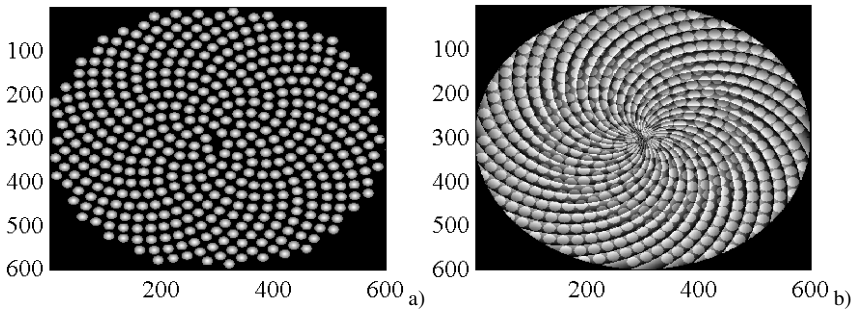

Fig. 2. Non-binary phase map superposed onto the PtDOE with different geometrical parameters a) φ =137.51° *n*=467 *c*=14 *r*=10, b) φ =137.51° *n*=467 *c*=14 *r*=11 *m*=34

3. Near-field diffraction pattern from the PtDOEs

To calculate the near-field diffraction pattern, it is considered a monochromatic plane wave of wavelength λ, normally illuminating the planar structure of the PtDOE situated at $z = 0$ (input plane), with the transmittance function given by the Eq. (2) for the binary or by the Eq. (3) for the non-binary phase distribution. The diffracted field, $U(x_0, y_0, z)$, at a distance z from the object (the output plane), can be expressed using the 2-D convolution operator [31]:

$$U(x_0, y_0, z) = t(x, y, 0) \otimes h(x_0, y_0, x, y, z), \tag{4}$$

where $h(x_0, y_0, x, y, z) = \dfrac{\exp(ikr_{01})}{i\lambda r_{01}}$ is the impulse response function, x_0, y_0 are the coordinates in the output plane, $k = 2\pi / \lambda$ and r_{01} is the distance between any two points from the input plane to the output plane. This equation is a direct consequence of the Rayleigh-Sommerfeld theory and is valid in near-field, our interest region.

The input wave field is restricted to an entrance circular aperture with the radius R_i (i. e. $t(x, y) = 0$ for $\sqrt{x^2 + y^2} > R_i$) and the radial extent of the observed wave field at the output

plane is confined at an exit aperture with a radius R_0 (i. e. $U(x_0, y_0, z) = 0$ for $\sqrt{x_0^2 + y_0^2} > R_0$).

If $R_i + R_0 < |z| < \dfrac{k(R_i + R_0)^2}{8}$, the diffraction pattern is calculated in the Fresnel approximation where the impulse response function from the Eq. (4) becomes:

$$h(x, y, z) = \frac{\exp(ikz)}{i\lambda z} \exp\left\{\frac{ik}{2z}\left[x^2 + y^2\right]\right\}, \tag{5}$$

and the complex amplitude of the diffracted field is given by:

$$U(x_0, y_0, z) = \frac{\exp(ikz)}{i\lambda z} \exp\left[\frac{ik}{2z}\left(x_0^2 + y_0^2\right)\right] \int_{-\infty}^{+\infty}\int_{-\infty}^{+\infty} U'(x, y, 0) \exp\left[-i2\pi\left(x_0 x + y_0 y\right)\right] dxdy \tag{6}$$

$$\text{where} \quad U'(x, y, 0) = t(x, y, 0) \exp\left[\frac{ik}{2z}\left(x^2 + y^2\right)\right], \tag{7}$$

and $U(x_0, y_0, z)$ is the 2-D Fourier Transform (FT) of the envelope $U'(x, y, 0)$ at the spatial frequencies $f_x = x_0 / \lambda z$, $f_y = y_0 / \lambda z$ up to multiplicative amplitude and phase factors.

For the numerical evaluation, these functions are sampled at the Nyquist frequency and the Eqs. (6) and (7) are implemented in discrete forms using 2-D matrices and the Fast Fourier Transform (FFT) routines in MATLAB.

In this section it is discussed the diffraction pattern from the binary phase-only PtDOE and, in the next section it is investigated the diffraction pattern from different non-binary phases distribution superposed onto the PtDOE structure. The numbers on the following figures axis represent the number of pixels and the values are normalized between 0 (black) and 1 (white).

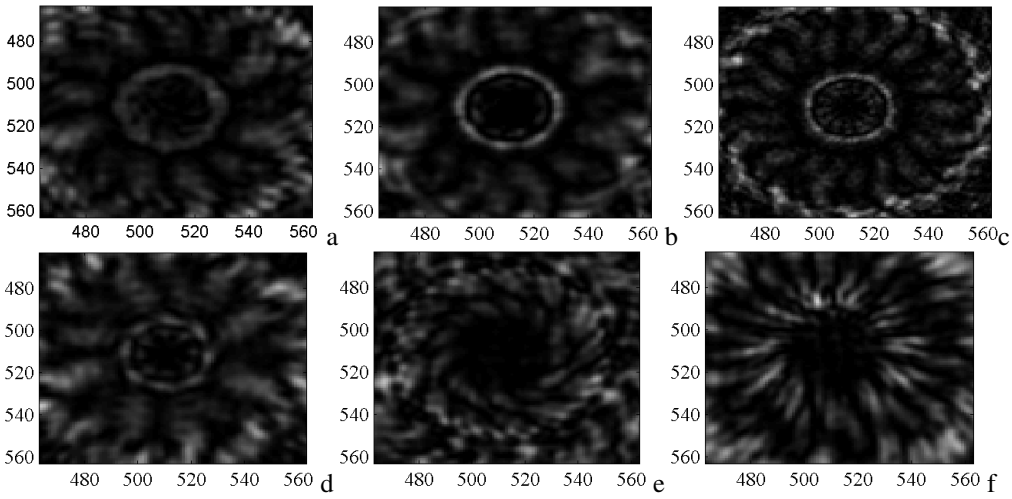

Fig. 3. Diffraction patterns at z = 40.0mm when the PtDOEs was generated with the following geometrical parameters a) φ =137.55° n=459 c=14 r=10, b) φ =137.51° n=467 c=14 r=12, c) φ =137.51° n=1414 c=8 r=6, d) φ =137.45° n=470 c=14 r=9, e) φ =137.45° n=401 c=15 r=11, f) φ =130.00° n=458 c=14 r=10

The dimensions of one pixel in the output plane are linked with the dimensions of one pixel in the PtDOE plane by the relations [32]:

$$N\Delta x\Delta x_0 = \lambda z \quad \text{and} \quad M\Delta y\Delta y_0 = \lambda z \tag{8}$$

where N, M are the numbers of pixels in the x, y directions, $\Delta x, \Delta y$ are the dimensions of one pixel in the PtDOE plane and $\Delta x_0, \Delta y_0$ are the dimensions of one pixel in the output plane.

The above equations are applied to calculate the diffracted intensity distribution from the PtDOEs depicted in Fig. 1. At the same $z = 40.0$mm, but for different geometrical parameters, the diffraction pattern has an annular symmetry with an almost zero intensity hole in its centre, but with confuse contour (see Fig. 3). Only for the PtDOE with an ideal arrangement (or closer), the transverse diffraction pattern has a central closed ring (CCR), with nearly zero intensity hole inside.

The simulations were performed for a large interval along the propagation axis in near-field. The evolution of the diffracted intensity distribution from the studied PtDOEs, exhibits a circular motion as it propagates along the optical axis. This property is exemplified here for the PtDOE generated with the parameters φ=137.51° n=323 c=17 r=11, and z between 60.5mm and 68.5mm with a step of 0.5mm (View the movie media1). As one can see in Fig. 4, the CCR from the diffraction pattern is clockwise rotated with 23.25°±0.01° when it is propagated along 0.8cm.

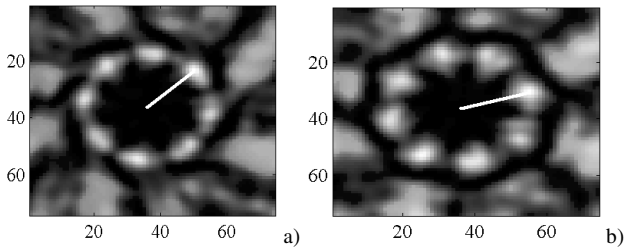

Fig. 4 The transverse diffraction patterns from the PtDOE generated with the parameters φ=137.51° n=323 c=17 r=11, at a) z = 60.5mm and b) z = 68.5mm

The self-focusing property of the intensity distribution in near-field, from a binary PtDOE is distinguished and illustrated here for a PtDOE structure generated with the φ=137.51° n=357 c=16 r=11. The propagation in the Fresnel approximation is simulated between $z = 55.0$mm and $z = 58.6$mm with an interval of 0.2cm between them, and the diffraction patterns are shown in the movie media2 and in Fig. 7 (for the first and the last image and for the one in the middle from the movie).

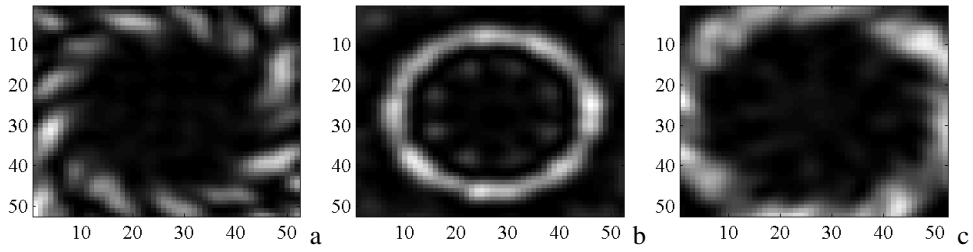

Fig. 5 The transverse diffraction patterns from a PtDOE generated with the parameters φ=137.51° n=357 c=16 r=11 at a) z = 55.0mm, b) z = 56.8mm, c) z = 58.6mm

If the PtDOE is generated with different geometrical parameters, the axial position, for the in focus CCR has different values. In Fig. 6 are shown the transverse diffraction patterns from the PtDOEs generated using the golden angle interval, but different filling intervals. This is an interesting property for a planar structure (no gray levels, convexity or concavity are present - easy to fabricate micro-relief).

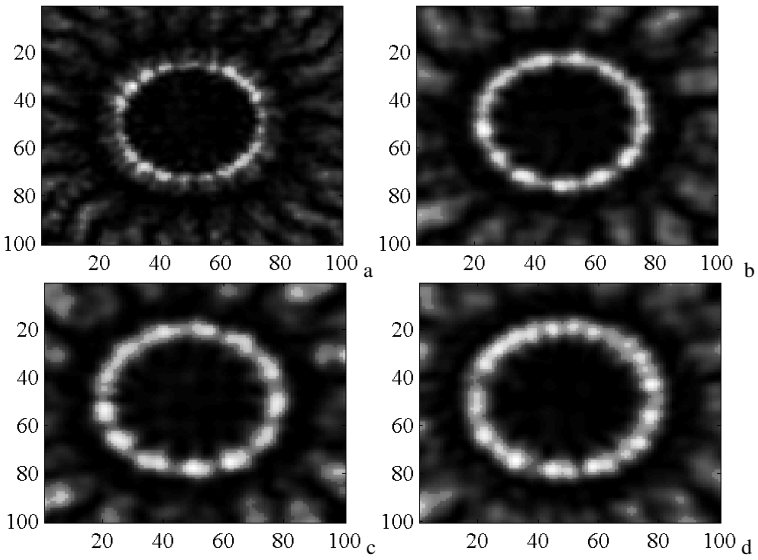

Fig. 6 Transverse diffraction patterns from the PtDOE generated with different geometrical parameters and the focalized CCRs are at different axial coordinate a) φ =137.51 c=8 r=6, z = 34.5mm b) φ =137.51, c=13, r=10, z = 39.4mm, c) φ =137.51, c=14, r=11, z = 44.3mm d) φ =137.51, c=15, r=11, z = 50.7mm

In Fig. 7 it is shown the evolution of the CCR diameter along the propagation axis, when the PtDOEs were generated with the same *r*, at different filling intervals, *c*. As one can see, the minimum values of the CCR diameter decrease with *c* and the in focus image appears at smaller values of the axial coordinate, z. These dependencies are in concordance with the Fig. 6.

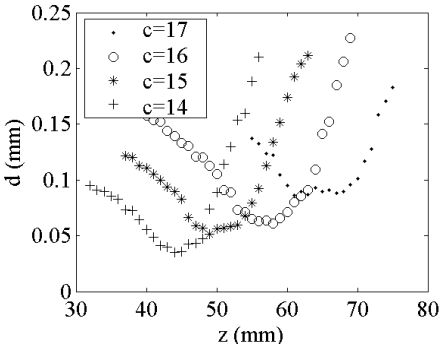

Fig. 7 The diameter evolution of the CCR when the PtDOE was generated with the same CE radius, *r*=11, but different filling intervals, *c*

The CCR diameter evolution when the PtDOEs were generated with the same *c*, but different *r*, is presented in Fig. 8. The CE radius has an insignificant influence on the position or the diameter of the CCR, at the same filling interval, *c*. In conclusion, we can say that the

self focusing property of the PtDOE generated after phyllotaxis geometry is given by the arrangement in spirals of the CEs, with the curvature depending on the filling interval, *c*.

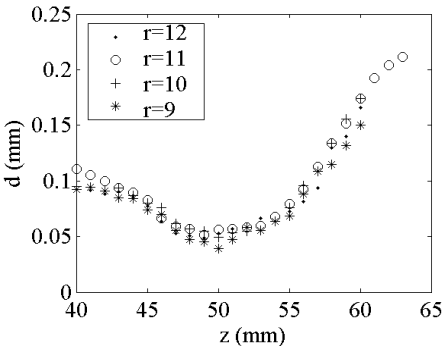

Fig. 8. The diameter evolution of the CCR when the PtDOE structures was generated with the same filling interval c=15, but different values for *r*

All these diffraction patterns from the PtDOE structure generated with the golden angle interval exhibit the same peculiarities: a central closed ring with the maximum intensity and nearly zero intensity inside the CCR, no matter the other geometrical parameters. For a binary phase distribution of phyllotaxis type, the diffracted intensity calculated in the Fresnel approximation presents two interesting properties: self-focusing and rotation along the propagation axis. One can obtain these two behaviors using a single PtDOE structure.

4. Non-binary phase distribution onto the PtDOEs structure

Different non-binary phase masks are superposed on the PtDOE structure to increase the intensity in the CCR and to decrease the unwanted noise. In Fig. 9, are shown the transverse diffraction patterns in different planes, perpendicular on the propagation axis from a PtDOE structure modulated by a helical phase distribution (like in the Fig. 2b).

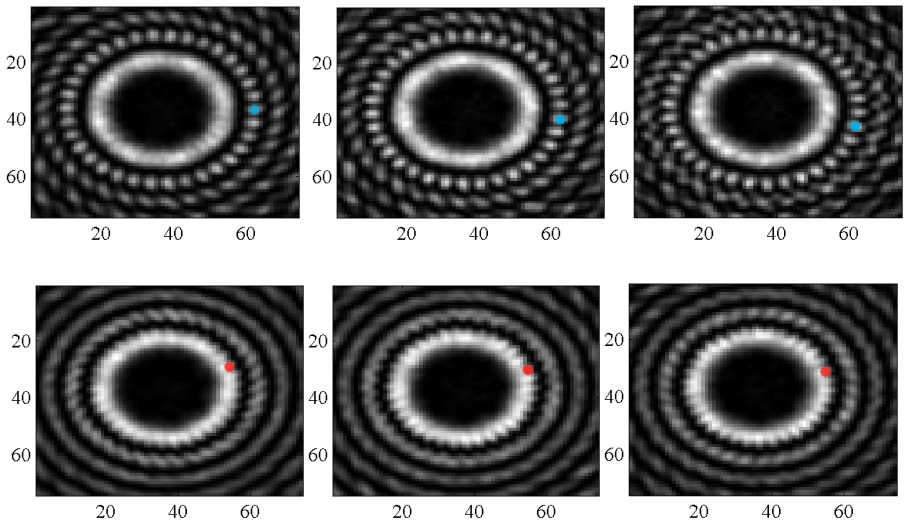

Fig. 9 The transverse diffraction patterns at a) z = 54.0mm, b) z = 56.0mm, c) z = 58.0mm, d) z = 68.0mm, e) z = 70.0mm, f) z = 72.0mm when we superposed a vortex on the PtDOE

The transverse diffraction patterns were computed for a PtDOE structure generated with the geometrical parameters $\varphi = \varphi_g = 137.51^o$, c=8 r=6 and a vortex with the topological charge m=34. The intensity and the uniformity in the CCR increase, besides the case when we have only the PtDOE structure. The intensity distribution after CCR is also in concentric rings which have a clockwise motion when it propagates along optical axis (see the blue and the red marks from the Fig. 9).

If the spirals from the vortex and the PtDOE structure have opposite orientations, the different rings have different senses of rotation. Some rings are present in the transverse diffraction patterns with anticlockwise motion and others with clockwise motion (see the Fig. 10, media3) as they propagate along the optical axis. The central hole with zero intensity is also present.

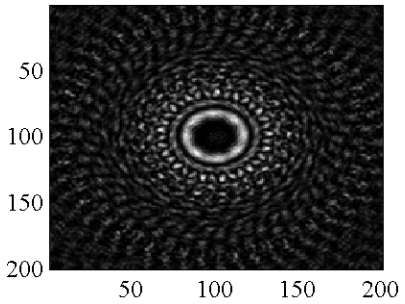

Fig. 10 Diffractive pattern from the PtDOE when an inverse vortex is superposed

In Fig. 11 it is shown the near-field diffraction pattern when a non-binary phase distribution of the micro-lens type is superposed on each CE arranged in the PtDOE structure. It exhibits the same peculiarity with the minimum central intensity. Compared with Fig. 6c, where the same geometrical parameters were used to generate PtDOE structure, here the uniformity inside the CCR and its intensity values increase. The surrounded noise decreases.

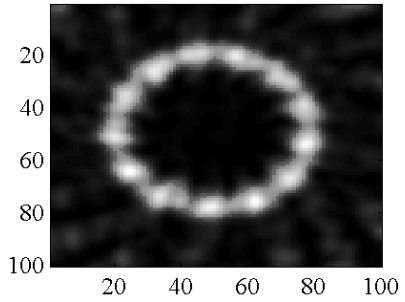

Fig. 11. The transverse diffraction pattern at z =41.8mm when the PtDOE structure was generated with the geometrical parameters: φ =137.51°, c=14, r=11, and a non-binary phase distribution of the lens type is superposed on each CE

In the above animated figures, each frame represents the transverse intensity distribution. They show the annular form of the transverse intensity, its self-focalization and also its rotation with the axial coordinate. All these features appear due to changes in the geometrical parameters of the phase-only diffractive element.

5. Conclusion

The near-field diffraction patterns from a quasi-periodic arrangement of the phyllotaxis type have been extensively analysed. The advantage of using a PtDOE as a diffractive structure lies in a large number of parameters (angle interval, filling factor, CE radius, CE number, non-binary phase), which can be changed to control the properties of the diffracted intensity.

Our results in the Fresnel approximation for a binary PtDOE show that its near-field diffraction pattern have a circular symmetry with a central closed ring and almost zero intensity inside. The geometrical parameters which generate the quasi-periodic arrangement of the phyllotaxis type influence these characteristics. The useful properties are the self-focalization and the rotation around the propagation axis of the diffracted intensity from a binary phase distribution (easy to fabricate planar microrelief, no gray levels, concavity or convexity are present). One can obtain these two behaviors using a single PtDOE structure.

For a proper non-binary phase functions applied on the PtDOE structure, the intensity in the diffraction pattern can be changed to reduce the surrounded noise, or to obtain the intensity distribution with concentric rings which have a rotational motion in opposite senses.

These properties will turn the PtDOE structure into an attractive geometry which can be used for beam shaping in the Fresnel approximation, for different research fields (diffractive optics, biology, optical tweezers, micro-pumps, micro-fluidics flow, viscosity studies).

Acknowledgements: The research has been (partially) supported by the Contract 4/CP/I/11.09.2007 PNCDI II "Capacities" and ANCS-UEFISCSU grant ID 1556 / 2009. I want to gratefully thank to Prof. A. M. Preda for the fruitful discussions.